water

MDPI

Article

Synergistic Remediation of Metal(loid)-Contaminated Groundwater Using Sequential BES–Phytoremediation Approach

Aqib Hassan Ali Khan [1,†], Martí Aliaguilla [2,†], Alberto Soto-Cañas [1], Diana Losantos [2], Carlos Rad [3], Carlos Rumbo [1], Sandra de la Parra [1], Blanca Velasco-Arroyo [4], Daniele Molognoni [2], Pau Bosch-Jimenez [2], Herwig De Wilde [5], Alfredo Pérez-de-Mora [6], Eduard Borràs [2,*] and Rocío Barros [1,*]

[1] International Research Center in Critical Raw Materials for Advanced Industrial Technologies (ICCRAM), University of Burgos, Centro de I+D+I, Plaza Misael Bañuelos s/n, 09001 Burgos, Spain; ahkhan@ubu.es (A.H.A.K.); asoto@ubu.es (A.S.-C.); crumbo@ubu.es (C.R.); sdelaparra@ubu.es (S.d.l.P.)
[2] Circular Economy & Decarbonization Department, Leitat Technological Center, C/de la Innovació 2, 08225 Terrassa, Spain; maliaguilla@leitat.org (M.A.); dlosantos@leitat.org (D.L.); dmolognoni@leitat.org (D.M.); pbosch@leitat.org (P.B.-J.)
[3] Research Group in Composting (UBUCOMP), Faculty of Sciences, University of Burgos, Plaza Misael Bañuelos s/n, 09001 Burgos, Spain; crad@ubu.es
[4] Department of Biotechnology and Food Science, University of Burgos, Plaza Misael Bañuelos s/n, 09001 Burgos, Spain; bvarroyo@ubu.es
[5] TAUW België nv, Department of Soil and Groundwater, Waaslandlaan 8A3, 9160 Lokeren, Belgium; herwig.dewilde@tauw.com
[6] TAUW GmbH, Department of Soil and Groundwater, Luise-Ullrich-Straße 14, 80636 Munich, Germany; alfredo.perezdemora@tauw.com
* Correspondence: eborras@leitat.org (E.B.); rbarros@ubu.es (R.B.)
† These authors contributed equally to this work.

Abstract

Conventional polluted groundwater remediation struggles with persistent metal(loid)s, creating a need for integrated bioelectrochemical systems (BESs) and phytoremediation. The proposed configuration consisted of two sequential BESs, a microbial fuel cell (MFC) followed by a microbial electrolysis cell (MEC), whose treated effluent and exhausted anolyte were subsequently polished in individual subsurface vertical-flow macrophyte mesocosms (VFMMs), planted either with *Phragmites australis*, *Scirpus holoschoenus*, or *Typha angustifolia*. The overall treatment period was 38 days, comprising 8 days of BES treatment followed by 30 days of VFMM treatment. With MFC-MEC pretreatment, an overall 91% metal(loid) removal efficiency (RE) was noted, with REs of >99% for Fe and Cu, and between 71% and 92% for Al, Ni, Zn, Cd, and As, significantly increasing groundwater pH from 2.66 to 4.65, at $p < 0.05$. Macrophyte mesocosms, notably with *P. australis* and *S. holoschoenus*, further reduced residual Cu, Cd, Zn, and As levels below Flemish groundwater sanitation standards, nutrient concentrations and ecotoxicity (as demonstrated by *Aliivibrio fischeri* bioluminescence assays). Residual Ni was reduced by >99.9% but remained above regulatory thresholds. BES–phytoremediation sequential integration proved to be an effective biotreatment that combines the rapid contaminant removal capacity of BES with the polishing and ecological stabilization functions of constructed wetlands.

Keywords: bioremediation; bioelectrochemical systems; phytoremediation; metals; groundwater

Check for updates

Academic Editor: Hodon Ryu

Received: 21 July 2026
Revised: 12 October 2026
Accepted: 14 October 2026
Published: 16 October 2026

Copyright: © 2026 by the authors. Licensee MDPI, Basel, Switzerland. This article is an open access article distributed under the terms and conditions of the Creative Commons Attribution (CC BY) license.

1. Introduction

High levels of metal(loid)s and extreme physical and chemical parameters in groundwater pose significant threats to both human health and the environment [1]. This issue can be further exacerbated in places where environmental regulation and sustainable practices have not been historically adopted. The effects of these pollutants on ecosystems are equally concerning, disrupting plant and animal life through unintended bioaccumulation, and altering vital water chemistry [2]. Thus, groundwater contamination can severely limit its suitability for drinking, irrigation, and other essential purposes, putting further pressure on already stressed water resources [3,4]. In addition, the introduction of metal(loid)s into an aquifer, driven by water percolation through polluted soil strata or natural rock formations, recharge and discharge cycles, and shifts in physicochemical conditions, can impair natural attenuation processes and compromise groundwater quality, posing a long-term threat to this vital resource [5,6]. If the source of the contamination is anthropogenic, remediation can likely be performed (e.g., by in situ or ex situ green remediation techniques), while, if it is natural, the composition of strata first needs to be analyzed to identify the possibility of remediation and the suitable intervention [5,7]. Therefore, there is an urgent need to address these challenges by identifying and mitigating pollution sources, implementing effective treatment strategies, and raising public awareness of the risks associated with metal-contaminated water [6,8].

The use of advanced green biotechnologies for the treatment of metal(loid)s has been intensely investigated for the remediation of environmental compartments and contaminated matrices [7]. Among the many different bio- and nature-based solutions used, phytoremediation and bioelectrochemical systems (BESs) are of great interest [9]. Phytoremediation utilizes plants and associated microorganisms that can perform the removal of pollutants. In this matter, numerous aquatic plants are reported to be promising for the remediation of polluted groundwater, with selection based on the target pollutants, the remediation end point, and the desired outcomes. For instance, Velasco-Arroyo et al. [3] identified *Lythrum salicaria*, *Mentha aquatica*, *Scirpus holoschoenus*, and *Typha angustifolia* as suitable species for rhizostabilization (metal(loid) stabilization in the rhizosphere), while *Carex riparia*, *Cyperus longus*, and *Iris pseudacorus* were proposed for phytoextraction (accumulation of metal(loid)s in harvestable plant tissues).

While this biotechnological intervention has little to no environmental impact, its implementation in urban and industrial settings remains challenging. Thus, the long treatment periods required for achieving desired pollutant removal rates, together with the large areas needed for the treatment, limit its applicability in many growing cities where land is scarce and expensive [10]. BES-based technologies have also emerged as a promising approach for the remediation of metal(loid)s in water, enabling effective removal of target metals at relevant remediation rates while achieving favorable outcomes [9]. BESs operate by harnessing the metabolic activities of microorganisms [11,12]. As microbes degrade organic matter, they transfer the electrons from respiration to the conductive material of an anode. These are then transferred though an external electric circuit to the cathode, where they are used to supply the necessary reductive power to perform metal(loid) precipitation, adsorption, and removal by complex formation. Further in, they can also be implemented in situ, and operated continuously on renewable energy, while offering the potential to recover the metal and metalloids [13].

The nature of contamination of groundwater can cause hindrance in the biological treatment activities. Furthermore, none of the remediation techniques are solely a perfect solution and capable of removing all contamination, without having limitations. Consequently, integrated treatment systems that combine multiple bio-based and nature-based remediation approaches can offer a more robust and versatile solution than their individual

application, as they can exploit the complementary strengths of each technology while mitigating their respective limitations [14,15]. The integration of BESs and phytoremediation is one of such promising strategy [16]. Despite the increasing interest in combining BESs and phytoremediation for environmental remediation, most previous studies have focused on hybrid configurations, such as plant microbial fuel cells, and constructed- and floating-wetland MFCs, in which electroactive processes and plant-based treatment occur within the same treatment compartment [17–21]. These studies have demonstrated that plant-derived exudates, root-associated microbial activity, and electrode-mediated redox processes can act synergistically to support pollutant removal and low-power generation. However, the sequential integration of BESs and phytoremediation, as distinct but complementary stages, remains comparatively underdeveloped.

Such decoupling may provide important operational advantages by enabling each technology to be operated under conditions optimized for its specific function [16,22]. In particular, high contaminant concentrations and salinity in water can limit the selection, establishment and performance of adequate plant species for phytoremediation [3]. Using BESs as a pretreatment step can reduce the contaminant load and toxicity reaching the wetland, potentially improving plant establishment, biomass production, and overall treatment performance [16,23]. Moreover, separating the BES from the phytoremediation stage enables operation under both microbial fuel cell (MFC) and microbial electrolysis cell (MEC) modes, providing complementary electrochemical conditions for the selective removal of metal(loids) [19]. MEC operation further introduces the additional electrochemical driving force required to target metal(loid)s that are more recalcitrant under spontaneous MFC operation [24]. The resulting process streams, including the treated catholyte and exhausted anolyte, can be further polished in subsurface vertical-flow constructed wetlands, thereby further exploiting the treatment capacity of the different technologies [16].

In this study, a novel sequential remediation train consisting of a two-stage BES, an MFC followed by an MEC, coupled to a subsurface vertical-flow constructed wetland was investigated for the treatment of acidic groundwater contaminated with metal(loid)s. *Phragmites australis*, *Scirpus holoschoenus*, and *Typha angustifolia* were selected for the macrophyte-assisted phytoremediation mesocosm system (MAPS) based on their metal(loid) phytostabilization and tolerance capacity screening against polluted groundwater [3,15,25]. This configuration aims to enhance overall metal removal while promoting a more circular and resource-efficient treatment approach. Accordingly, this study aimed to (i) quantify metal(loid) removal and overall treatment performance across the integrated setup, (ii) evaluate the toxicological profile of the treated water and its effects on macrophyte health, and (iii) assess the feasibility and potential scalability of combining complementary bioelectrochemical and nature-based technologies for sustainable groundwater remediation.

2. Materials and Methods

2.1. Polluted Groundwater Collection and Characterization

Polluted groundwater (PW) was collected from a historic metallurgical industrial site located in northern Flanders (Belgium), with a long history of metallurgical activity dating back to the 19th century. Due to confidentiality agreements associated with the EU Projects GREENER (Grant 826312) and BIOSYYMO (Grant 101060211), the exact location of the site cannot be disclosed. The site geology is characterized by a sequence of alternating permeable Quaternary and Tertiary sands and fine sands, interbedded with locally occurring low-permeability clay layers. Additional details on the geology and hydrogeology of the site are provided in [26]. For the present study, a total of 100 L of groundwater was collected in February 2024 from a single groundwater monitoring well (8101), selected as

representative of the groundwater affected by the metal(loid) contamination and acidic conditions. The well is screened at a depth of 8–9 m below ground level, within the uppermost permeable fine sand layer (second aquifer). This aquifer is confined by non-permeable clay layers approx. 3–4 m thick above and below the screened interval. Groundwater was sampled using low-density polyethylene tubing positioned at the target depth and connected to a surface-mounted peristaltic pump (12 VCD Advanced, EijkelkampSoil & Water, Giesbeek, The Netherlands).

Sampling was performed by standard low-purging rate (0.10–0.15 L min^{-1}). Field parameters (pH, electrical conductivity, redox potential and dissolved oxygen) were monitored during purging via a calibrated multi-sensor (Horiba, Kyoto, Japan). The groundwater had a pH of 2.7 and exhibited an electrical conductivity (EC) of 5.3 dS m^{-1}. The metal(loid) concentration (in mg L^{-1}) was as follows: Al 374.4, Ni 186.6, Cu 264.0, Fe 316.3, Zn 98.1, As 1.4, and Cd 2.5. The corresponding threshold values (in µg L^{-1}) were 40 for Ni, 100 for Cu, 200 for Fe, 500 for Zn, 20 for As, 5 for Cd, and 20 for Pb [27]. All measured concentrations exceeded these threshold values. This specific polluted groundwater was selected as a representative benchmark of severe, complex legacy contamination typical of historic European metallurgical and chemical industrial sites. Concentration limits were benchmarked against Flemish groundwater standards (VLAREBO), which represent the regional legally binding implementation of the EU Groundwater Directive (2006/118/EC; 2026/805/EC) tailored to local hydrogeology and environmental risk management.

2.2. Integration of Sequential BESs with Phytoremediation Wetlands

PW was treated using an integrated system combining bioelectrochemical systems (BESs) with macrophyte-assisted phytoremediation. In the first stage, PW was subjected to BES treatment first in a microbial fuel cell (MFC) reactor and subsequently in a microbial electrolysis cell (MEC) reactor. In the second stage, a mixture containing the BES-treated groundwater and exhausted acetate mineral media from the BES reactors was fed into the phytoremediation mesocosms. The schematic design of combined BESs and phytoremediation is presented in Figure 1A. Detailed descriptions of the BES reactors and wetland mesocosms, together with the operational parameters applied at each stage, are provided in Sections 2.2.1 and 2.2.2.

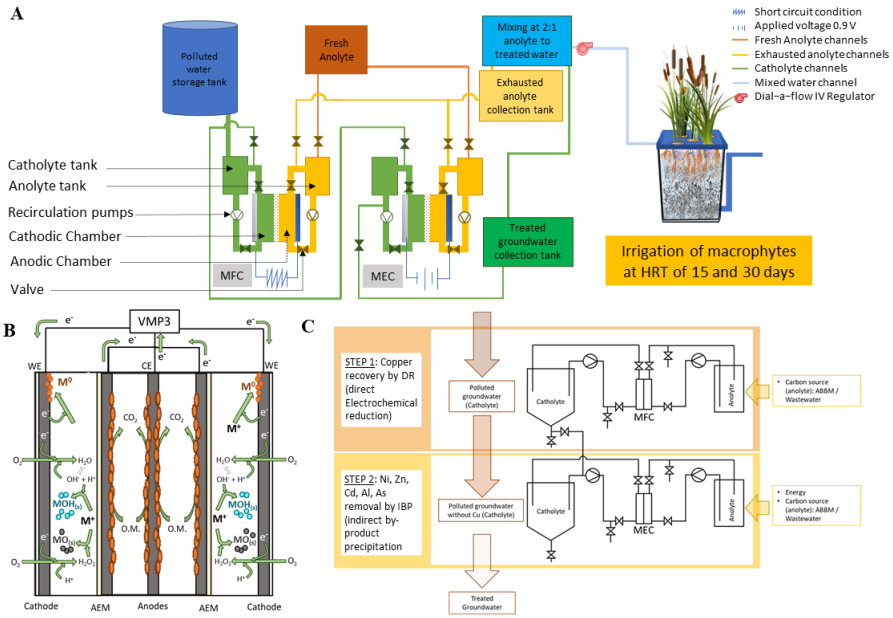


Figure 1. Experimental concept used for metal(loid) removal in polluted groundwater. (**A**) Scheme of the setup using BESs coupled to phytoremediation (arrows in the corresponding streams showing

the direction of flow, while valves were used to prevent the different streams from mixing when the PW and anolyte were moved between MFC and MEC); (**B**) design of pilot-scale BES reactors with biotic anodes and abiotic air cathodes, with expected reactions during operation (green arrows). O.M. = organic matter, CO_2 = carbon dioxide produced upon utilization of OM, AEM = anion exchange membrane, P.S = power source, e^- = electrons being transported through an external electric circuit from the anodic chambers to the cathodic ones, WE = working electrode, CE = counter electrode, M^+ = metal ions dissolved in groundwater, M^0 = elemental (zero-valent) metals electrodeposited on the cathode surface, $MO_{(s)}$ = metal oxide precipitates formed in the reactor due to oxygen reduction reactions, $MOH_{(s)}$ = metal hydroxide precipitates formed in the reactor due to oxygen reduction reactions; and (**C**) sequential operation of BES reactors for decontamination of polluted water.

2.2.1. BES Operation and Design

Two pilot-scale BES reactors were designed and constructed at LEITAT facilities, following the scheme of Figure 1B. Each reactor was composed of four chambers, including two anodic chambers located in the middle of the reactor and two cathodic chambers positioned at the opposite ends. Each anodic chamber was equipped with two planar anodes made of 100 cm^2 of carbon felt (SGL group, Hvidovre, Denmark). The anodes were previously inoculated in separate single-chamber BESs using a mixed culture sourced from the effluent of a long-term operating microbial fuel cell [28].

The inoculum was mixed at a 1:1 (v/v) ratio with acetate-based mineral medium (ABMM; composition provided in the Supplementary Information). The reactors were operated in step-batch feeding mode, with a 30 s feeding period followed by 3570 s without feeding, corresponding to a feeding rate of 80 mL day^{-1}. To ensure reproducible bioanode development and functional activity, electrostimulation was conducted under a 3-electrode configuration by progressively modulating the anode's potential in a controlled gradient from −0.10 V to −0.35 V vs. Ag/AgCl (3M KCl) in −0.05 V increments, over a total enrichment period of 22 days [29]. Active bioanode establishment and functional reproducibility were verified by achieving stable, steady-state current generation at each applied potential step, finally achieving a current density of $\geq$0.1 mA cm^{-2} prior to transitioning the system to the acidic groundwater matrix.

The cathodic chambers were each equipped with an air-cathode, allowing both electrodeposition and indirect by-product precipitation due to oxygen reduction reactions (ORRs), as shown in Figure 1B. The air-cathode was designed with unidirectional carbon fibers (100 cm^2 surface, SGL Carbon) painted with 2 mg cm^{-2} of an ORR catalyst (PMF-011904; Pajarito Powder, Albuquerque, NM, USA) as cathode and a hydrophobic textile (Tyvek; Dupont, Wilmington, DE, USA) placed on the external side, acting as a water impermeable layer and an air diffusion membrane. Both cathodic chambers were separated from the central anodic chambers by anion exchange membranes (AEMs). For this purpose, AMI-7001 (Membrane International, Ringwood, NJ, USA) was used. In addition, stainless-steel current collectors were situated in both anodic and cathodic chambers. Throughout operation PW was used as the catholyte, while ABBM was used as the anolyte. The cells were hydraulically operated in batch mode, recirculating the solutions in their respective chambers by the help of peristaltic pumps at a flowrate of 10 L h^{-1}. For the MFC reactor, 2.4 L of PW was treated during a 4-day batch cycle.

The effluent from the MFC was then transferred to the MEC and treated for an additional 4-day batch cycle (see Figure 1C). In each reactor, 4.8 L of acetate mineral medium was continuously recirculated. Specific details of design parameters used for the BES reactors are presented in Table 1.

Table 1. Design parameters of BES reactors used for the experiment.

Parameter	Pilot Reactor
Surface ratio (cathode vs. anode)	1:2
Cathode surface	200 cm^2
Anode surface	400 cm^2
Catholyte volume vs. cathode surface ratio	12 mL/cm^2
Volume ratio (catholyte vs. anolyte)	1:2

Regarding electrochemical operation, the MFC reactor was operated by connecting an external resistance between the electrodes, while the MEC reactor was operated in a two-electrode configuration, by controlling the cell voltage at 0.9 V, by means of a power source (72-2715; TENMA, Leeds, UK). To better understand the metal(loid) removal dynamics under this MFC+MEC configuration, samples were collected from the catholyte solutions every 24 h, for metal(loid) quantification and physicochemical characterization. Metal(loid) removal efficiency and rate as well as cathode coulombic efficiency were analyzed using the equations described next.

The removal efficiency (R_{EF}) was calculated using the following equation:

$$R_{EF}(\%)=\frac{C_0-C_F}{C_0}$$

where C_0 represents the initial and C_F represents the final metal concentration in g L^{-1}.

The removal rate (R_R) was calculated as

$$R_R=\frac{\Delta C_M \times V}{Q \times t}$$

where ΔC_M is the change in metal concentration in the catholyte (g L^{-1}); V is the catholyte volume in L; Q operating in batch mode is equivalent to the catholyte volume in m^3; and t is the experiment time in days.

The cathode coulombic efficiency (CE_{CAT}) was calculated as

$$CE_{cat} = \frac{F \times n \times V_{cat} \times \Delta C_M}{M_M \times \int Idt}$$

where F is the Faraday constant (96,500 C·mol^{-1}), n is the molar number of electrons required for metal reduction (mol·mol^{-1}), V_{CAT} is the catholyte volume (L), ΔC_M is the change in metal concentration in the catholytes (g·L^{-1}), M_M is the molecular weight of the removed metal (g mol^{-1}), I is the current in A and t is the time in s.

2.2.2. Experimental Conditions for Wetland Mesocosms

In the second stage, the BES-treated groundwater was mixed at a 1:2 ratio with a 50:50 blend of the exhausted anolytes collected from the MFC and MEC reactors and the resulting mixture was subsequently fed into the phytoremediation mesocosms. A total of 3 different species of emergent macrophytes were used, including *Phagmites australis*, *Scirpus holoschoenus*, and *Typha angustifolia* (provided by Viveros La Dehesa, Valdeobispo, Spain). The plants were acclimatized and cultivated at 28:16 °C and photoperiods of 16:8 h light: dark conditions [15].

During the acclimatization period, for each species, 3 plants (~1 month old) of homogenous size per pot were maintained for 2 weeks, before being exposed to the mixture of BES-treated groundwater + exhausted anolyte. Two HRTs (15 and 30 days) were selected, and mesocosms for each treatment and HRT were prepared independently, with three

biological replicates per treatment. The HRTs were selected based on prior experimental optimization and exposure regime studies [3,25]. In addition, control plants of each species were cultivated under identical conditions but without exposure to the contaminated groundwater–anolyte mixture at both HRTs. Standalone phytoremediation control treatments (macrophytes exposed directly to polluted groundwater without bioelectrochemical pretreatment) and unplanted matrix controls (gravel-only mesocosms receiving BW) were omitted to avoid redundant experimentation, as these baseline matrix adsorption, abiotic precipitation dynamics, plant tolerance capacities, and hydraulic retention dynamics were already established and validated in prior studies using identical plant species and water matrices [3,15,25,30]. The experiment was conducted for a total of 30 days.

Square polypropylene pots were used for the experiments, having dimensions of 195 mm width, 195 mm length, and 190 mm height. Each pot was filled with fine gravel (range 4–24 mm, D50 = 14.0 mm) previously sieved and washed with water to remove rock debris (<4 mm). The porosity of the gravel used in the system was 38.97%, while the specific yield from the system was 33.46%, and the specific retention was 5.51%. These parameters indicate that, among the total void space of 38.97%, upon filling of the wetland system, a total of 5.51% water is retained on gravel while the 33.46% was freely available. Flowrates (Q, ml day^{-1}) of 78 and 39 were applied to retain HRTs of 15 and 30 days, respectively. Each wetland pot was equipped with inlet and outlet hydraulic structures to maintain the desired water level and hydraulic conditions. The inlet consisted of a 100 mL syringe connected with a Plastic dial-a-flow IV Infusion Set Micro Drip Regulator (SaniBur, Burgos, Spain), allowing precise control of the irrigation flowrate. The system outlet was located at an orifice in the pot equipped with a bulk-head captive joint connected to a pneumatic male cylinder rotating elbow, which was elevated at about 175 mm (just below the upper surface of the gravel levels in the pots), and connected using PTFE tubing. The end of the tubing was fitted with a pneumatic shut-off valve, to prevent draining of the pot wetland system. Overflow water was collected every 15 days for metal content analysis. A constant water volume of 3.5 L was maintained throughout the experiment to prevent plant dehydration stress and ensure adequate sample collection.

2.3. Physiological Parameter of Harvested Macrophytes

After 30 days of treatment, macrophytes were harvested from each pot. The fresh and dry biomass of both roots and shoots for all the plant species was quantified gravimetrically and expressed as mean values (g ± SD). For fresh biomass, the samples were weighted immediately after harvesting, while for dried biomass, plant tissues were weighed after drying at 60 °C (till the constant weight was achieved). The dried biomass of shoot and root, along with the growth substrate (soil), was further analyzed for metal(loid) content. In addition, the water storage capacity of the plant tissues was calculated from the difference between fresh and dry biomass and expressed as g g^{-1} dry biomass using the following equation:

$$Water\ storage\ capabilty = \frac{Fresh\ weight - Dry\ weight}{Dry\ weight}$$

2.4. Quantification of Metal(loid)s in Water, Plant, and Soil Samples

Upon receipt, contaminated groundwater was characterized to verify the concentrations of the target metal(loid)s and establish the baseline composition of the water matrices under study. In addition, as specified in Sections 2.2.1 and 2.2.2, water samples collected throughout the treatment period from the MFC, MEC, and phytoremediation systems were analyzed and quantified. These samples were centrifuged (at 4000× g for 10 min), filtrated

(using Scharlau CF/WASH110 filter paper Ø 110 mm; Scharlab, S.L, Spain), and acidified using (1:9 *v*:*v*) concentrated HNO_3, prior to quantification [30].

Apart from water characterization assays, meta(loid) concentrations were determined in samples corresponding to shoot, root, and growing substrate (GS) collected from experiments at 15- and 30-day HRTs. The preparation of the samples prior to their quantification, i.e., the digestion protocols, was different depending on the target matrix. Plant and GS samples were firstly dried at 60 °C until constant weight and subsequently subjected to acid digestion with 2 mL of 33% *v*/*v* H_2O_2 and 8 mL of 65% concentrated HNO_3 in a microwave oven (ETHOS ONE; Millestone, Shelton, CT, USA), for 20 min at 190 °C [3,15]. For quality assurance, rye grass-certified standard material (ERM-CD281), soil standard (BCR-483), and blanks were included in digestion batches. The final digested solutions were filtered using Scharlau CF/WASH110 filter paper (Ø 110 mm) and brought to a final volume of 50 mL with deionized water. Major and trace elements in both digested extracts and water samples were quantified using inductively coupled plasma optical emission spectrometry (ICP-OES; GENESIS, SPECTRO, Kleve, Germany) operated in radial view mode and inductively coupled plasma tandem mass spectrometry (ICP-MS/MS; 8900 Triple Quadrupole, Agilent Technologies, Santa Clara, CA, USA).

2.5. Determination of Physicochemical Parameters in Water Samples

Physicochemical parameters of the water samples were measured using a multiparameter probe (HI98194; Hanna Instruments, Italy), for simultaneous determination of pH, electrical conductivity (EC), redox potential (ORP), and total dissolved solids (TDSs) [25]. Between measurements, the probe was carefully washed with distilled water to avoid cross-contamination. In addition, nutrient levels were monitored in samples collected after 15 and 30 days of treatment, under both HRTs. A segmented flow chemical analyzer (San++; SKALAR, Breda, The Netherlands) was used for the determination of ammonium, nitrites, and phosphates, according to Berthelot, Griess-Ilosvay, and Murphy & Riley methods, respectively [15]. The calibration standards were prepared using a DOSIMAT automatic dispenser (Metrohom, Herisau, Switzerland).

2.6. Toxicity Assessment Using the A. fischeri Bioluminescence Inhibition Assay

The ecological impact of the integrated system for metal(loid) remediation was assessed by studying the changes in the pattern of bioluminescence produced by *A. fischeri* [31]. Microtox assays were performed in triplicate for each mesocosm under the different macrophyte and HRT conditions. The bacterial suspension was prepared using individual *A. fischeri* colonies exhibiting the highest bioluminescence. The suspension was subjected to centrifugation at 3600 *g* for 15 min, and the resulting pelleted cells were resuspended in 5 mL of NaCl 2% (*w*/*v*) and maintained at 10 °C for 30 min. Opaque 96-well microplates were prepared containing 90 µL of water samples (polluted and clean), collected at the end of the experiment and resuspended in a 2% NaCl solution. In addition, positive (219.8 mg/L of $ZnSO_4 \cdot 7H_2O$ in 2% NaCl) and negative controls (2% NaCl) were prepared. Later, 10 µL of the bacterial suspension was added, and bioluminescence was immediately measured to determine the initial peak value using a microplate reader (BioTek, Synergy HT; Agilent, Santa Clara, CA, USA) at 490 nm. After initial peak value determination, the plate was incubated in a Thermomixer at 800 rpm and 15 °C, and changes in the bioluminescence of *A. fischeri* were recorded in the microplate reader at 5 min intervals for 30 min.

2.7. Statistical Analysis

Means and standard deviations were computed for each variable using a minimum of three independent experimental repetitions. Data normality and homogeneity of vari-

ances were assessed using the Kolmogorov–Smirnov and Levene tests, respectively, with treatment serving as the fixed factor. The data was examined using ANOVA, with a significance level of $p < 0.05$. The treatments were subsequently contrasted using Duncan's post hoc tests. All statistical analyses were performed using the Statistical Package for Social Sciences (SPSS v22.0 for Windows) and JASP (v0.17.1).

3. Results

3.1. BES Performance in Sequential Treatment

BES performance was assessed in terms of metal(loid) removal efficiencies, as shown in Figure 2. The sequential MFC+MEC strategy achieved an overall metal(loid) removal efficiency of 91%, compared with 38% after the MFC stage alone, demonstrating the complementary role of the two BES configurations (Figure 2A). In the MFC step, Cu and Fe were significantly removed, with both metals accounting for removal efficiencies higher than 99.8%, while As was also significantly removed (90%). The subsequent MEC treatment further enhanced the removal of the remaining contaminants, achieving final removal efficiencies of 92%, 87%, 76%, and 71%, for Al, Cd, Zn, and Ni, respectively. The evolution of metal(loid) concentrations throughout the treatment is shown in Figure 2B. Consistent with their high removal efficiencies during the MFC stage, As, Fe and Cu concentrations decreased rapidly, reaching values close to complete removal within the first 50 h of operation. Conversely, Al, Ni, Zn, and Cd concentrations remained relatively stable during the MFC phase and were primarily removed during MEC operation, during which, their concentration progressively declined, until the end of the treatment.

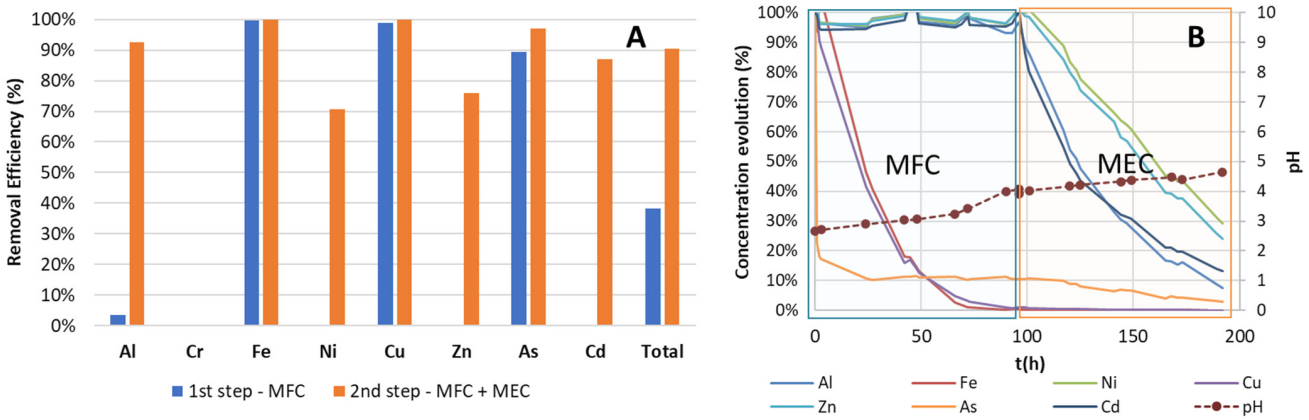


Figure 2. BES performance for metal(loid) removal using a sequential MFC and MEC treatment. (**A**) pollutant removal efficiencies achieved during each stage of the sequential treatment. (**B**) Metal(loid) concentration and pH evolution throughout the sequential treatment.

The sequential treatment also resulted in a gradual increase in catholyte's pH, from an initial value of 2.66 to 4.06 after the MFC stage, and 4.65 following MEC treatment. This progressive pH increase most likely contributed to the partial removal of Al during the MFC stage, and its near-complete removal during the MEC phase (Figure 2B), particularly considering the highly negative reduction potential required for the electrochemical reduction in Al, which was not reached under the applied operating conditions. The average current density was 1.2 A m^{-2} during the MFC operation and increased to 1.9 A m^{-2} during MEC operation. The cathodic coulombic efficiency reached 273% during the MFC stage and 104% during the MEC stage. Values exceeding 100% suggest that the observed metal removal could not be solely attributed to electrochemical reduction. Instead, the co-occurrence of additional physicochemical conditions, particularly the precipitation and co-precipitation of metal oxides and hydroxides, affects the overall removal efficiency.

Figure 3 shows the deposits formed on the cathode surfaces and the precipitates accumulated in the buffer tanks after the different treatment steps. Clear differences were observed in the appearance of the deposits between each stage. The cathode from the MFC step was predominantly covered by reddish-brown deposits (Figure 3A), likely corresponding to zero-valent Cu, whereas the MEC cathode exhibited whitish precipitates, which may be associated with Ni and Zn- containing compounds. The orange-brown sludge observed in the buffer tank (Figure 3B) was hypothesized to be associated with iron precipitates, consistent with the tendency of this metal to precipitate under the prevailing pH conditions. In contrast, the whitish, gelatinous precipitates observed after the MFC stage (Figure 3C) are likely predominantly associated with aluminum hydroxides. This interpretation is in agreement with the sequential Al removal pattern shown in Figure 2B and the progressive increase in pH throughout the treatment. During operation, a decrease in the activity of electroactive biofilms was observed after several treatment batches. In some cases, the biofilm electroactivity was inhibited by 70–90%. This inhibition may be associated with the characteristics of the treated groundwater and the accumulation of sulphates in the anolyte, when trespassing the anionic exchange membrane, affecting biofilm performance.

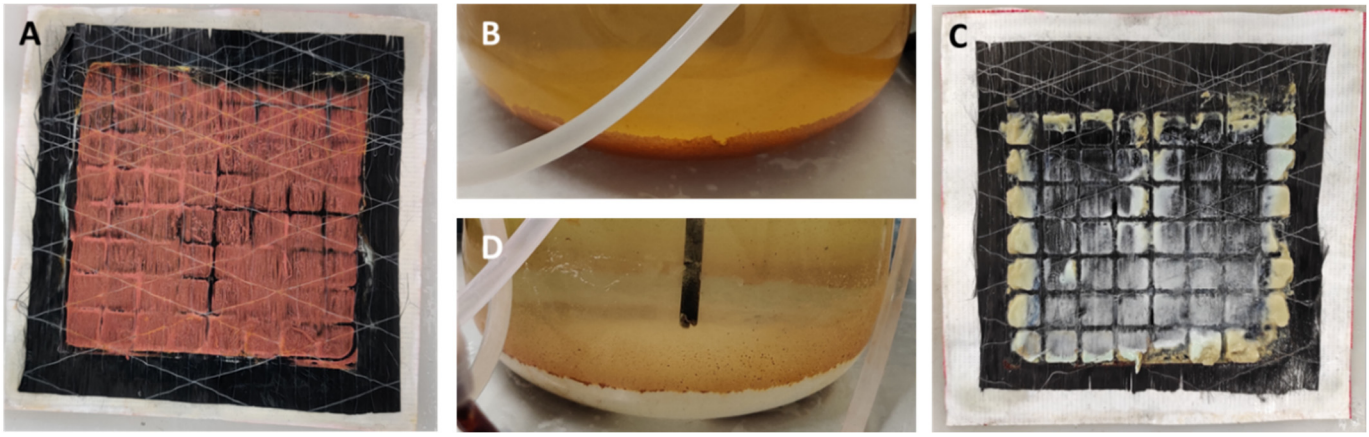


Figure 3. Physical appearance of cathodes and accumulated precipitates after treatment phases. (**A**) Cathode after MFC treatment of groundwater, (**B**) precipitate sludge accumulated in the buffer tank during MFC experiment, (**C**) cathode after MFC+MEC treatment, and (**D**) precipitate sludge accumulated in the buffer tank during MEC experiment.

3.2. Macrophyte Performance in Wetland Mesocosms Irrigated with Treated Water

The concentration of metal(loid)s in BW (the mixture of BES-treated water and exhausted anolyte), which was used for phytoremediation mesocosm irrigation, was as follows: Al 22.5, As 0.1, Cd 0.3, Cu 0.5, Fe 0.6, Ni 52.6, and Zn 23.5. The BW was supplied to the macrophyte mesocosms at a controlled flowrate using a dial-a-flow IV Infusion Set Micro Drip Regulator, as seen in Figure 4A. No evident differences in overall plant phenotype were observed between plants irrigated with clean water (CW) and those irrigated with BW (Figure 4B). However, *P. australis* irrigated with BW developed a noticeably larger canopy cover than plants receiving CW throughout the experimental period, suggesting a species-specific response to the irrigation conditions.

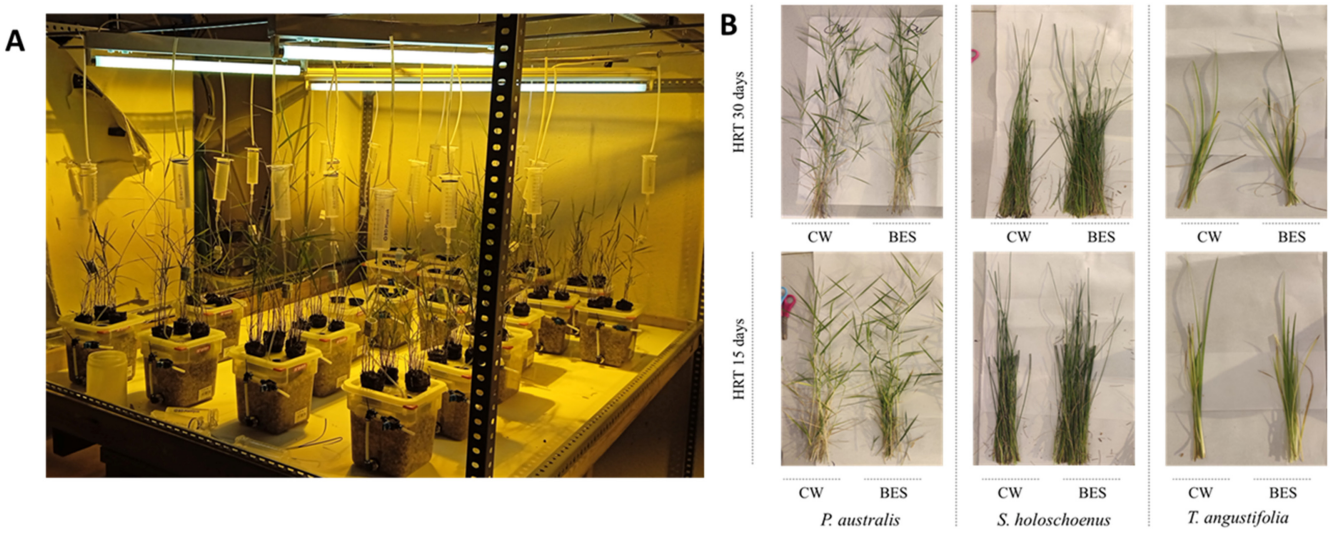


Figure 4. Wetland mesocosms irrigated with BW. (**A**) *P. australis* mesocosm setup used for the experiment, (**B**) harvested canopy status at HRTs of 30 and 15 days, for *P. australis*, *S. holoschoenus*, and *T. angustifolia*, respectively.

In contrast, at harvest, biomass production showed a significant increase under BW irrigation, with both *P. australis* and *S. holoschoenus* exhibiting higher biomass than their respective CW controls. Nevertheless, this increase was statistically significant only for *Scirpus holoschoenus*, which produced significantly greater biomass when irrigated with BW compared to the corresponding CW control (Table 2). In addition, most biomass-related parameters showed no significant differences regardless of the hydraulic retention time (HRT) applied (15 or 30 days).

Table 2. Physiological parameters of macrophytes irrigated with BES-treated water mixed with anolyte (BW).

Parameter		HRT	*Phragmites australis*		*Scirpus holoschoenus*		*Typha angustifolia*	
			CW [1]	BW [1]	CW	BW	CW	BW
Shoot	FW (g)	30	12.50 ± 1.12	14.21 ± 2.25	11.97 ± 0.76	24.25 ± 3.40 *	10.34 ± 0.10	9.64 ± 0.48 [a]
		15	13.21 ± 1.15	14.10 ± 1.67	12.41 ± 0.98	26.52 ± 1.54 *	12.34 ± 0.19	9.64 ± 0.96 [a]
	DW (g)	30	1.98 ± 0.59 *	2.26 ± 0.87 *	2.14 ± 0.05 *	2.26 ± 0.02 *	0.52 ± 0.05 [a]	2.76 ± 0.10 *
		15	1.05 ± 0.16	1.17 ± 0.08	2.07 ± 0.02 *	2.40 ± 0.05 *	0.46 ± 0.05 [a]	2.32 ± 0.11 *
	WSC ($g\ g^{-1}$)	30	10.52 ± 0.52	11.96 ± 1.38	9.57 ± 0.71	22.18 ± 3.38 *	9.82 ± 0.05	6.88 ± 0.38 [a]
		15	12.16 ± 0.99	12.93 ± 1.59	10.27 ± 0.93	24.26 ± 1.52 *	11.88 ± 0.14	7.32 ± 0.85 [a]
Root	FW (g)	30	4.86 ± 0.89	5.12 ± 1.26	7.18 ± 1.15	11.45 ± 2.11 *	4.99 ± 0.54	4.25 ± 0.51 [a]
		15	4.65 ± 0.51 [a]	5.63 ± 0.91	7.98 ± 1.02	12.14 ± 2.12 *	5.65 ± 0.19	4.56 ± 0.41 [a]
	DW (g)	30	1.10 ± 0.45	1.01 ± 0.24	3.48 ± 0.17 *	3.57 ± 0.14 *	0.74 ± 0.10 [a]	0.87 ± 0.24
		15	1.21 ± 0.24	1.17 ± 0.17	3.37 ± 0.45 *	4.17 ± 0.50 *	0.69 ± 0.06 [a]	0.73 ± 0.05
	WSC ($g\ g^{-1}$)	30	3.76 ± 0.44 [a]	4.11 ± 1.02	3.70 ± 0.97 [a]	7.88 ± 1.98 *	3.38 ± 0.27 [a]	4.25 ± 0.44
		15	3.44 ± 0.27 [a]	4.46 ± 0.74	4.61 ± 0.57	7.97 ± 1.62 *	3.83 ± 0.36 [a]	4.96 ± 0.14

Notes: [1] CW is clean water, while BW is BES-treated water + exhausted anolyte mixture. [a] indicates the significantly lower results, while * indicates the significant differences between treatments at $p < 0.05$.

While only a few differences with reference to different applied HRTs were observed, including in CW-irrigated *T. angustifolia*, the fresh shoot biomass (10.34 ± 0.10 at 15 days HRT, and 12.34 ± 0.19 for 30 days HRT, respectively) and water storage capacity (9.82 ± 0.05 at 15 days HRT, and 11.88 ± 0.14 for 30 days HRT, respectively) were found to vary significantly, and when aggregated with BW, the *T. angustifolia* also showed statistically

significant variation in shoot dried biomass (2.76 ± 0.10 at 15 days HRT, and 2.32 ± 0.11 at 30 days HRT, respectively). When comparing the same HRT with different irrigation regimes, the fresh biomass production and water storage capacity of root and shoot for *P. australis* and *S. holoschoenus* were significantly better in plants irrigated with BW.

3.3. Metal(loid) Accumulation in Macrophyte Root and Shoot of Root

Among all the studied metal(loid)s (Al, Cd, Cu, Fe, Ni, and Zn), tissue accumulation predominantly occurred in the roots rather than in the shoots, indicating the phytostabilization was the primary mechanism involved in the retention of these elements (Figure 5). An exception was observed for As and Cd uptake. Arsenic showed negligible accumulation in the roots compared with the shoots of *P. australis* and *S. holoschoenus*, whereas Cd was preferentially translocated to the shoots, particularly in *T. angustifolia*. Metal(loid) accumulation in plant tissues was influenced by the residual concentrations present in the BW, as well as by contributions from the growth substrate, including the potting soil and gravel used in the experimental setup. Reducing the hydraulic retention time (HRT) from 30 to 15 days significantly enhanced root accumulation in BW-irrigated plants, especially in *T. angustifolia* and *S. holoschoenus*. At the 15-day HRT, root concentrations of Al, Cu, Fe, Ni, and Zn were significantly higher than those observed at the 30-day HRT.

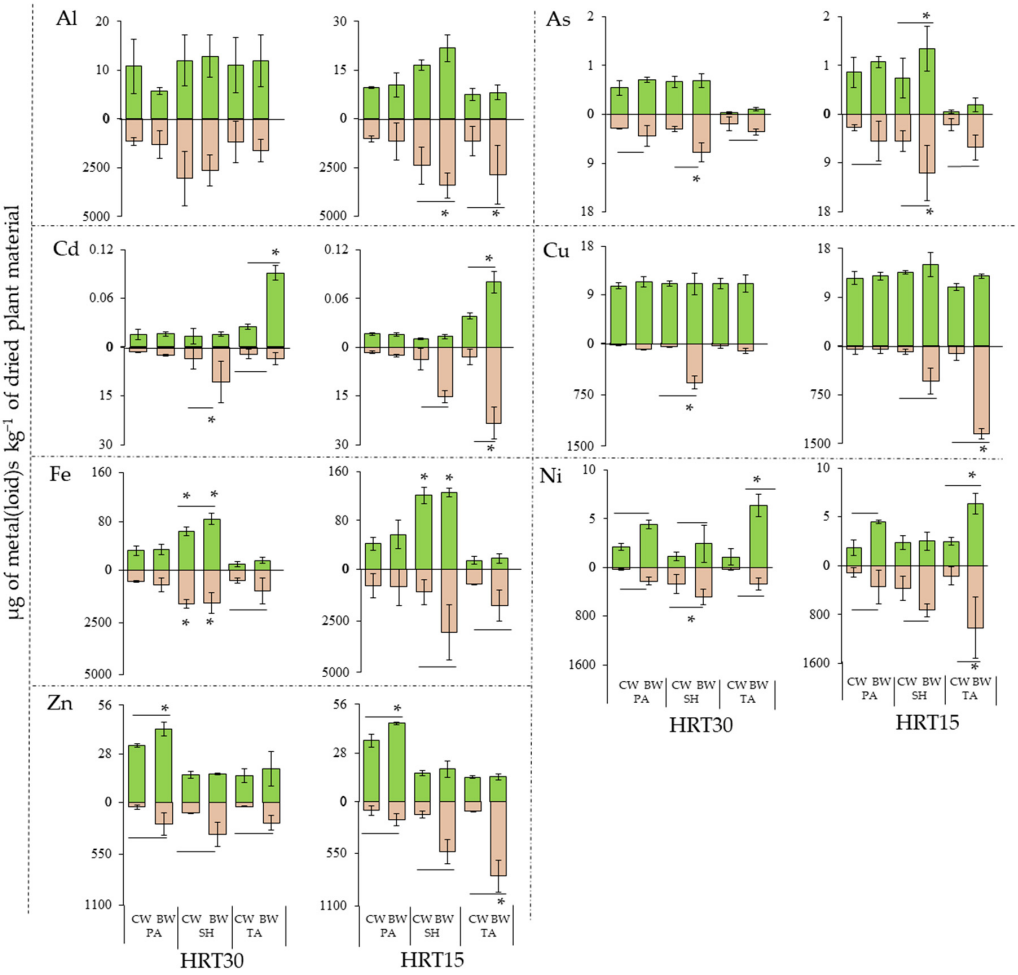


Figure 5. Metal(loid)s uptake in macrophytes irrigated with BW at different HRTs. Green bar represent metal(loid)s in shoot and beige color bar represent metal(liod)s in root. The asterisk (*) on the bar indicates a significantly higher level detected between the specific treatments (CW or BW) within the root or shoot. Lines between bars of CW and BW indicate a significant difference detected in root or shoot for a specific plant.

In contrast, shoot accumulation remained stable between the two retention times, indicating that the shorter HRT primarily impacts and accelerates the rhizofiltration and sequestration dynamics taking place at the root–water interface. Species-specific accumulation patterns were also noted in the metal(loid) content uptake. *P. australis* exhibited a notable capacity for Zn accumulation in the aerial part, at both HRTs. Conversely, the accumulation profiles of Fe, Cd, and Ni in shoot and root remained relatively low and stable across treatments. *S. holoschoenus* showed higher uptake of Fe and Al in both root and shoot compared to the other macrophytes, at both HRTs. Furthermore, at HRT15, it displayed a significant increase in both root and shoot accumulation for Al and As when exposed to BW. *T. angustifolia* accumulated significantly higher aboveground levels of Cd and Ni across both retention times. In addition, when irrigated with BW, this species showed significantly greater root accumulation of Cd, Cu, Ni, and Zn than the other macrophytes. This effect was further enhanced at the 15-day HRT, where root concentrations of these elements were significantly higher than those observed at the 30-day HRT.

3.4. Metal(loid) Concentrations in Wetland Mesocosm Outflow

The profile of metal(loid) levels in water after 15-day (T1) and 30-day (T2) time intervals with different studied HRTs is presented in Figure 6. Significant reductions in BW metal(loid) concentrations were achieved at both hydraulic retention times (15 and 30 days), with final concentrations falling below the permissible limits defined by the Groundwater Sanitation Standards of Flanders, for most of the studied metals and metalloids. The sequential treatment system is as follows. BES pretreatment, followed by macrophyte mesocosm for polishing treated groundwater and exhausted anolyte, achieved significant overall removal across all evaluated metal(loid)s, compared with initial industrial concentrations (Figure 6).

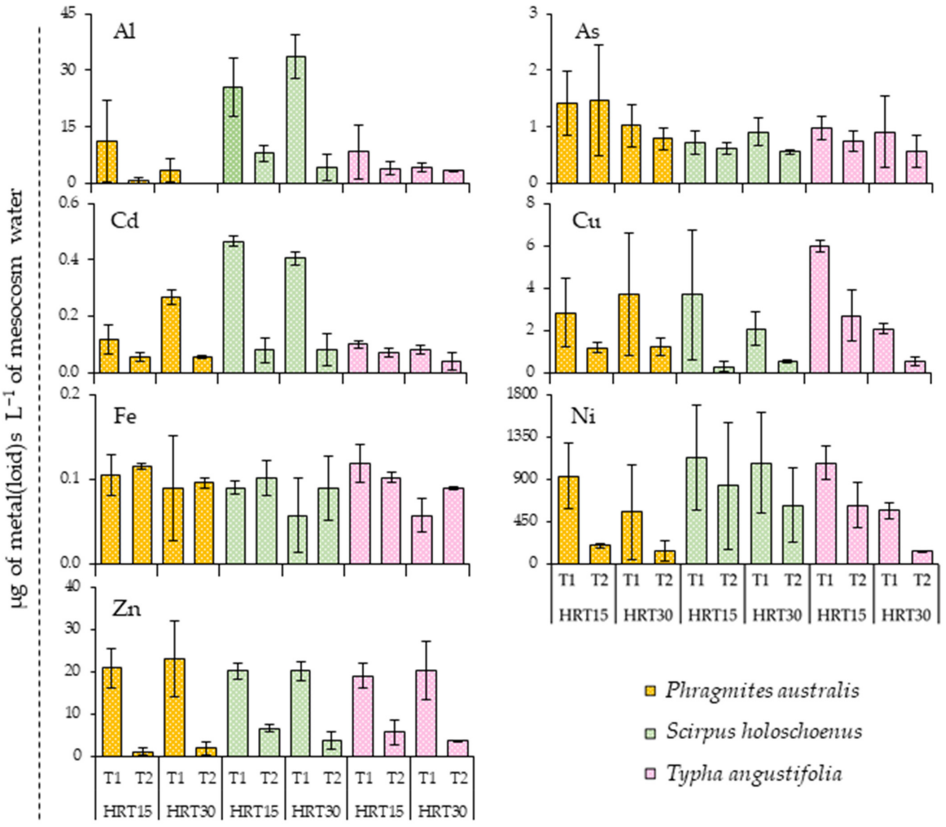


Figure 6. The water metal(loid) profile in macrophyte mesocosms irrigated with BW at T1 and T2 (on the 15th and 30th days of exposure) with both studied HRTs.

Final concentrations for Cu, Cd, Zn, and As successfully met Flemish regional groundwater standards (VLAREBO). For nickel, the T2 treatment regime achieved >99.9% removal compared to the raw groundwater (186,600 μg L^{-1}), with final levels reaching 144.11 ± 96.53 μg L^{-1} and 135.91 ± 1.73 μg L^{-1}, on T2 with HRT30, for *P. australis* and *T. angustifolia* mesocosms, respectively. Despite this >3-log attenuation, residual Ni concentrations in T2 water remained above the 40 μg L^{-1} VLAREBO regulatory threshold, indicating that nickel was the most recalcitrant metal in the polluted groundwater. The extent of metal(loid) removal varied slightly according to the macrophyte species, hydraulic retention time, and the individual metal(loid). Furthermore, increasing the exposure duration within each HRT led to additional decreases in metal(loid) concentrations, demonstrating the continued capacity of the macrophytes to remove residual contaminants from BW.

The most notable trend across the analyzed metal(loid)s (Al, Cd, Cu, Ni, and Zn) was the significant progressive reduction in concentrations over time. Concentrations at T1 were consistently higher than those measured at T2. Regardless of the macrophyte species or HRT applied, metal(loid) concentrations generally decreased over time, indicating the continued removal of residual contaminants during the treatment period. Exceptions to this are noted with As and Fe, exhibiting highly stable, low-level concentrations with overlapping levels, indicating that neither treatment type, plant species, nor HRT alters their dynamics.

Species-specific differences were particularly evident at T1, when residual metal(loid) concentrations were highest. *S. holoschoenus* (green) mesocosms demonstrate having significantly higher concentrations of Al and Cd, with Al levels peaking significantly at HRT30. Meanwhile, *T. angustifolia* (pink) displayed a spike in Cu concentrations, specifically at HRT15. *P. australis* (yellow) mesocosms, which showed slightly elevated Zn levels at HRT30 and relatively high As levels at HRT15 compared to the other species. The effect of HRT depended on the metal(loid) considered. For As, Fe, and Zn, increasing the HRT from 15 to 30 days produced only minor variations in concentration patterns. In contrast, more pronounced differences were observed for Al and Cu. For example, *S. holoschoenus* mesocosms exhibited higher residual Al concentrations at T1 under HRT15, whereas *T. angustifolia* demonstrated more effective Cu removal at HRT15 than at HRT30.

Mesocosms irrigated with BES effluent maintained an alkaline and strongly reducing environment across all tested macrophyte species; however, physical parameters shift dramatically depending on hydraulic retention time and exposure duration (Supplementary Table S1). Most notably, operating the system at a faster flowrate (HRT 15) for an extended 30-day period resulted in significant spikes in electrical conductivity, total dissolved solids (TDSs), and salinity (Supplementary Table S1). This significant ionic buildup corresponds directly with absolute minimums in internal electrical resistance and a slight decrease in the system's reducing potential. Interestingly, an inflection point exists where the ion accumulation under a slower flow (HRT 30) for 30 days exactly mirrors the accumulation seen under a faster flow (HRT 15) for just 15 days, highlighting a distinct time-flow dependency in the system's overall electrochemical dynamics.

The study demonstrated that increasing the hydraulic retention time to 30 days, in combination with phytoremediation using different macrophyte species, significantly reduced not only the residual concentrations of both metal(loid)s, but also the contents of PO_4, NH_4, and NO_3 (Table 3). For reference, the initial concentration (mg L^{-1}) of $NO_3{}^-$-N, $NH_4{}^+$-N, and $PO_4{}^{-3}$-P present in the polluted water with BES treatment was 0.4 ± 0.01, 6.8 ± 0.21, and 0.32 ± 0.07, respectively. However, when the polluted groundwater was mixed with the exhausted anolyte with a 1:2 ratio, changes in the levels were also noted. The $NO_3{}^-$, $NH_4{}^+$, and $PO_4{}^{-3}$ level (mg L^{-1}) in BW reached 0.03 ± 0.01, 0.17 ± 0.05, and 25.05 ± 3.59, corresponding to a ~92.5 to 97.5% reduction in $NO_3{}^-$ and $NH_4{}^+$ levels,

while there was a ~98.7% increase in levels of the PO_4^{-3}. The substantial increase in phosphate concentration was attributable to the composition of the exhausted anolyte used to prepare the BW mixture. Elevated phosphate levels in treated effluents may pose an environmental risk, as they can promote eutrophication and algal blooms in receiving water bodies. Consequently, the ability of the different macrophyte species to further reduce nutrient concentrations was evaluated, and the results are presented in Table 3.

Table 3. Primary dissolved water nutrients at studied HRTs (15 and 30 days) with different selected plants.

Parameters [1]	HRT	*P. australis*		*S. holoschoenus*		*T. angustifolia*	
		CW	BW	CW	BW	CW	BW
NO_3^--N	30	0.14 ± 0.03 *	0.01 ± 0.01 [a]	0.10 ± 0.02	0.03 ± 0.02	0.05 ± 0.03	0.07 ± 0.01
	15	0.07 ± 0.02	0.04 ± 0.02 [a]	0.15 ± 0.03 *	0.05 ± 0.01 [a]	0.06 ± 0.02	0.09 ± 0.06 *
NH_4^+ -N	30	0.13 ± 0.01	0.06 ± 0.01 [a]	0.24 ± 0.19	0.50 ± 0.14 *	0.25 ± 0.05	0.18 ± 0.04
	15	0.22 ± 0.08	0.12 ± 0.01 [a]	0.16 ± 0.05	0.46 ± 0.01 *	0.27 ± 0.06	0.46 ± 0.05 *
PO_4^{-3}-P	30	0.24 ± 0.01 [a]	10.20 ± 0.22	0.34 ± 0.09	18.10 ± 0.39 *	0.45 ± 0.33	15.78 ± 0.23 *
	15	0.05 ± 0.01 [a]	35.62 ± 1.62 *	0.10 ± 0.01 [a]	37.58 ± 0.93 *	0.07 ± 0.01 [a]	34.75 ± 1.14 *

Notes: [1] The parameters (mg L^{-1}) were assessed on the 30th day of treatment with both HRTs. [a] indicates the significantly lower, while * indicates the higher, level(s) of the studied parameter at different HRTs.

The response of nitrate levels to different HRTs varied significantly between the water types (CW vs. BW) and plant species. At a longer retention time (HRT = 30 days), BW consistently exhibited lower concentrations compared to CW across all species, with *P. australis* achieving the lowest levels. Reducing the retention time to 15 days led to an increase in NO_3^- concentrations within the BW systems, most notably in *T. angustifolia* (0.38 ± 0.06). For CW, the 15-day HRT generally resulted in lower residual nitrate concentrations than the 30-day HRT across all species. Ammonium concentrations showed distinct patterns based on species selection and HRT. For *P. australis*, doubling the HRT from 15 to 30 days effectively reduced the levels in both CW and BW. *S. holoschoenus* and *T. angustifolia* maintained relatively high NH_4^+ concentrations in BW regardless of the HRT, with *S. holoschoenus* displaying a high variance at 30 days (0.50 ± 0.14) and both species stabilizing around 0.46 mg L^{-1} at a 15-day HRT.

Despite these differences, both nitrate and ammonium concentrations remained well below the discharge limits commonly established for treated wastewater, indicating effective nitrogen removal by the integrated treatment system. At an HRT of 30 days, residual nutrient concentrations were significantly higher in BW treated with *Scirpus holoschoenus* and *Typha angustifolia* than in *Phragmites australis* mesocosms. Conversely, at an HRT of 15 days, phosphate concentrations increased across all BW-irrigated macrophyte mesocosms, suggesting that extending the HRT is necessary to improve phosphate (PO_4^{3-}) removal.

3.5. Assessment of *A. fischeri* Bioluminescence Inhibition

The bioluminescence of *A. fischeri* reduced almost at the start of the experiment as soon as the bacteria encountered polluted groundwater (Figure 7). The assay confirmed the sensitivity of *A. fischeri* to the $ZnSO_4 \cdot 7\ H_2O$, made evident by a rapid and continuous drop in bioluminescence, from an initial value of ~15,000 arbitrary units (a.u.) to near-zero levels, by the 30th min of exposure. With polluted water, the instant decline to zero level was noted for *A. fischeri*, which indicates the extreme acute toxicity, as seen in Figure 7. Groundwater only treated with BESs resulted in constant lower bioluminescence (around

10,000 a.u. at the start of the exposure and dipping down toward 8000 a.u. by the end of the assay).

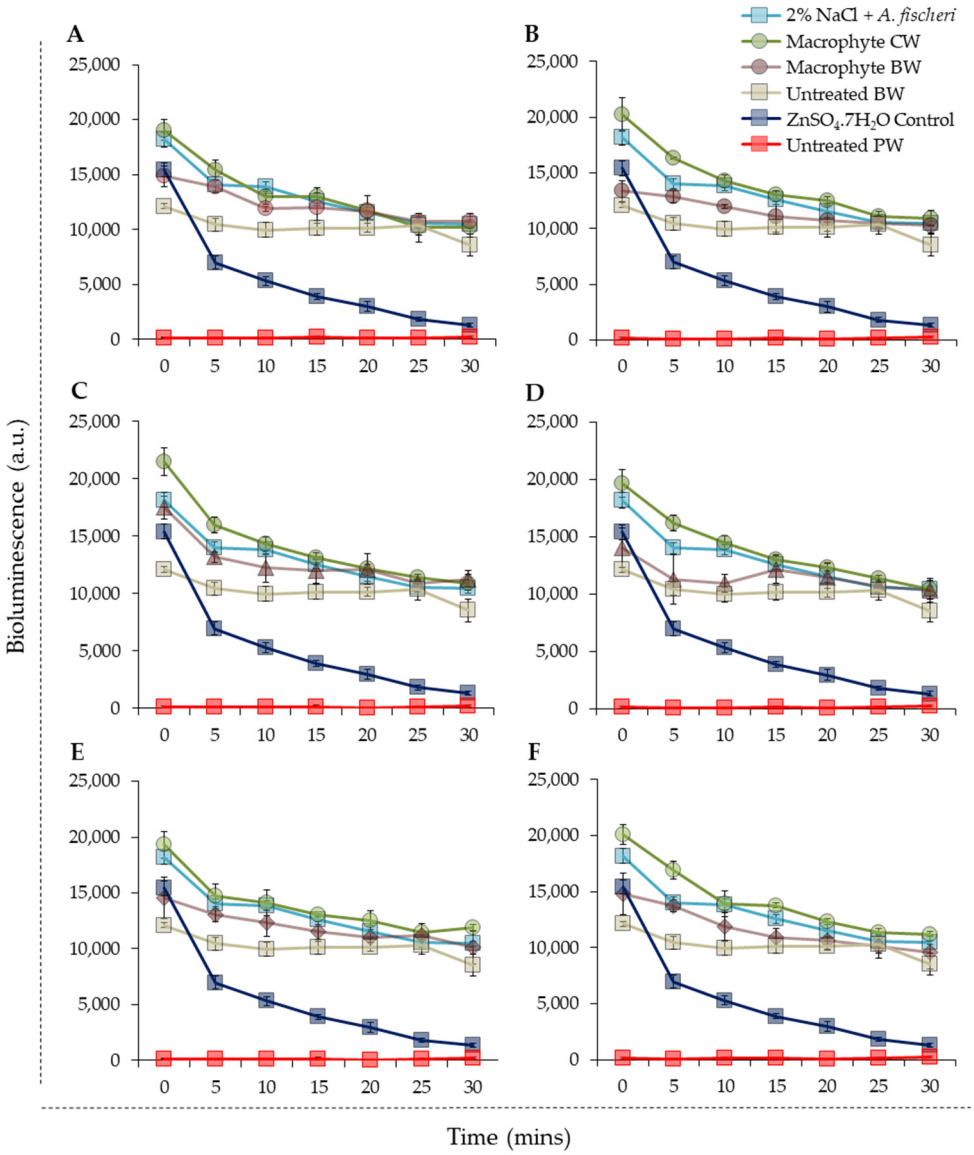


Figure 7. *A. fischeri* bioluminescence assay with macrophyte mesocosm irrigated with BW at HRT 15 and 30 days, respectively, presented in (**A**,**B**) for *P. australis*, (**C**,**D**) for *S. holoschoenus*, and (**E**,**F**) for *T. angustifolia*.

The combined treatments (BES + phytoremediation) showed improvement in the bioluminescence compared to only BES treatments; there is a drop in the initial bioluminescence peak, until a time point of 5 to 10 min, where the levels of bioluminescence are similar to those of the 2% NaCl + *A. fischeri* control. Across both HRTs and with all macrophytes (*S. holoschoenus*, *T. angustifolia*, and *P. australis*), an improved and non-toxic profile for bioluminescence was noted that was comparable with the control treatment, which was irrigated with clean water.

Extending the HRT from 15 to 30 days resulted in a significant improvement in retaining *A. fischeri* bioluminescence for BW treated in *P. australis* and *T. angustifolia* mesocosms; however, by 25 min, no differences in bioluminescence between treatments were observed, followed by a decrement in untreated BW treatment. It indicates that the co-application of BESs and phytoremediation showed considerable reduction in the toxicity level. The

negative impact of faster HRT (15 days) was also evident in combined treatment, where, compared to the control, the toxicity was higher.

4. Discussion

The use of individual bio- and nature-based solutions for water remediation can be beneficial. However, most of the polluted matrices are heterogeneously contaminated, often containing different types and concentrations of multiple contaminants at varying concentrations. As a result, relying on a single NbS approach may be overly ambitious and insufficient to achieve remediation objectives [14]. In addition, multiple factors can limit the effectiveness of standalone NbS applications, including treatment endpoints, remediation time, operational and optimization constraints, and challenges associated with large-scale implementation [10,23,32]. In the present work, the integration of BESs with phytoremediation was assessed to reduce metal(loid)s in polluted groundwater. Particular emphasis was placed on reducing metal(loid) concentrations while simultaneously minimizing secondary pollution associated with residual contaminants in the treated effluent and exhausted process streams, such as the spent anolyte generated during BES operation.

The two-stage BES treatment of polluted groundwater with MFC followed by MEC resulted in an overall removal efficiency of 91% for cumulative metal(loid)s, which was attributed to the removal of Cu and Fe (up to ~90%) in the MFC reactor, while Al, Cd, Zn, and Ni were also significantly removed in the subsequent MEC reactor. The observed element-specific removal pattern, with rapid elimination of Fe and Cu in the MFC stage and later removal of Al, Ni, Zn, and Cd in the MEC stage, agrees with the literature and suggests that BES performance depends on potential pathways that include a combination of physical, chemical, and bioelectrochemical processes, which are linked with metal speciation, redox behavior, reactor configuration, and achieved operational parameters [13,33]. The high Cu removal observed in this study is consistent with previous reports describing Cu as one of the most readily recovered metals in BESs, given its positive standard reduction potential (0.13 V vs. Ag/AgCl 3M), while Fe is often removed efficiently through a combination of electrochemical reduction and precipitation processes [34,35]. In contrast, the comparatively slower but still substantial Ni and Zn removals are also consistent with BES studies indicating that these metals usually require longer treatment times or stronger electrochemical driving forces to achieve higher conversion rates [36]. Similar findings were reported by Modin et al. [37], which demonstrated the sequential recovery of metals based on their thermodynamic reduction potentials in BESs, and showed that, while elements like Cu and Fe can be recovered spontaneously, metals with lower standard reduction potentials like Zn^{2+} require a significantly stronger electrochemical driving force (higher applied voltage) and specific potential control to achieve reduction, which is why MEC operation was selected.

The coulombic efficiencies recorded during MFC and MEC operation were unusually high, providing additional evidence that contaminant removal was likely not driven only by direct electrochemical reduction [38]. Values above 100% have been reported in BESs treating metal-rich streams and are typically interpreted as evidence that multiple simultaneous processes contribute to contaminant removal, including precipitation, adsorption, and co-precipitation [39–41]. Direct electroreduction of species with positive reduction potentials, such as Cu, Fe, and As, probably contributed to their efficient removal in the first stage of the BES treatment [42,43]. However, the increase in pH from 2.66 in the influent groundwater to 4.06 after the MFC stage and 4.65 following MEC treatment likely also promoted the precipitation of metal oxides and hydroxides (expected, given the selected air-cathode reactor configuration), as well as the formation of insoluble metal-bearing

phases, a mechanism that has been well documented in bioelectrochemical and related electrochemical systems [22].

This removal mechanism is particularly relevant for metals with more negative reduction potentials, for which direct electrochemical reduction may not be favored under the operating conditions of the system, as in the case of Al [43,44]. Taken together, these results suggest a mixed mechanism in which redox transformations and chemical precipitation operated simultaneously. The visual appearance of the cathodes and the collected precipitates also supports this interpretation. The reddish deposits observed after MFC operation are consistent with the near-complete removal of Cu and with the formation of metal-rich surface deposits that are commonly reported in BES metal-recovery studies [37]. Likewise, the whitish deposits formed after MEC treatment are compatible with Zn- and Ni-bearing precipitates, which are frequently associated with cathodic alkalinization and hydroxide formation [45,46]. The orange-brown sludge accumulated in the buffer tanks is also consistent with extensive Fe precipitation, as reported in BESs and related electrochemical treatments of metal-contaminated waters [36].

From a technological standpoint, the sequential arrangement proposed in this work offers a relevant advantage over direct BES–phytoremediation integration [47,48]. Most studies combining BESs and plants have focused on simultaneous rhizosphere-based systems, where electrochemical and plant-mediated processes occur in the same unit [23,49]. While such approaches can be highly efficient, balancing the physicochemical conditions to maintain both electrochemical performance and plant-microbiome health remains a key optimization challenge [9,50]. In contrast, using BESs as a first conditioning step reduces the pollutant load before the wetland stage, improving plant establishment and operational flexibility [10,48].

A critical limitation observed during BES operation was the sharp decline in electroactive biofilm activity (70–90%) observed after successive treatment cycles. Since the metal-contaminated groundwater was confined to the cathodic compartment, and the AEM limited the transport of metal cations to the anolyte, this decline cannot be directly attributed to metal toxicity toward the anodic biofilm [51]. Instead, it is likely associated with changes in anolyte composition resulting from the transport of anionic species across the AEM [52]. In particular, the migration and subsequent accumulation of sulfate in the anolyte may have contributed to the observed decrease in bioelectrochemical activity during prolonged treatment [53]. Continuous anolyte renewal at an appropriate flowrate could help limit sulfate accumulation and maintain favorable conditions for electroactive biofilm activity [50,54]. Several operational and reactor-design strategies could eventually be considered for addressing this limitation and protecting the anodic biofilm. Alternatively, reactor configurations incorporating an additional chamber or ion-exchange membrane could provide greater control over ion transport and further protect the anodic compartment [55,56].

From a practical engineering perspective, the observed decline in bioelectrochemical output indicates that standalone BES units in their current form need improvement for a successful long-term field operation [41,46,54]. However, this limitation does not undermine the intrinsic potential of the proposed sequential BES–VFMM architecture strategy. Rather, the present results identify a specific operational challenge that can guide future reactor optimization, while demonstrating the potential of the BES to serve as an intensive primary stage designed for rapid acute toxicity reduction and bulk metal stripping, thereby shielding the downstream macrophyte wetland from severe chemical shock [17,21,52]. Addressing this issue will be important for improving operational stability and for advancing the scale-up potential of the proposed treatment scheme [33,35]. Furthermore, as this study was performed in batch mode, future investigations should focus on continuous-flow sys-

tems to support the practical implementation and scale-up of this integrated NBS for aquatic remediation. Such studies should explore various BES configurations, reactor designs, and operating conditions in combination with macrophyte-assisted phytoremediation.

The enhanced biomass production observed for *Phragmites australis* and *Scirpus holoschoenus* exposed to BES-pre-treated groundwater provides functional evidence of reduced acute phytotoxicity and successful plant acclimatization to the treated groundwater, as raw and untreated groundwater, characterized by extreme acidity and high metal(loid) loads, can severely impair macrophyte growth [15,30]. Furthermore, this increased biomass may indirectly contribute to treatment performance by enhancing nutrient uptake, aerating the rhizosphere, and fostering microbial communities potentially involved in the immobilization and phytostabilization of residual metal(loid)s within the wetland substrate, rather than relying solely on direct hyperaccumulation in plant tissues [3,10]. Overall metal(loid) removal from water in subsurface vertical-flow systems is also dependent on abiotic and biotic interactions, which include physical filtration, adsorption onto substrate surfaces, chemical precipitation, substrate microbial activity, and macrophyte-assisted rhizofiltration and phytostabilization [15]. Based on the findings in the present study, it can be proposed that the sequential configuration combining the high treatment efficiency of bioelectrochemical systems with the ecological stabilization and polishing capacity of macrophyte-assisted phytoremediation is beneficial for treating metal(loid)-polluted water. However, further studies should also include unplanted substrate controls to quantitatively distinguish the relative contributions of plant uptake/rhizofiltration versus abiotic substrate adsorption and precipitation.

The decrease in residual toxicity, measured with the *Aliivibrio fischeri* assay, confirms that the treatment train not only reduced chemical concentrations but also improved ecological quality [31]. *A. fischeri* and related luminescence-based assays are widely used to detect remaining toxicity in waters contaminated by metals and metalloids, because chemical removal does not always guarantee biological detoxification [15]. In this study, the reduction in toxicity after BESs and phytoremediation indicates that the combined process mitigated both dissolved contaminant burden and overall biological stress. This is an important result because biological assays often reveal residual effects of secondary or intermediate contaminants formed after treatment that are not evident from concentration data alone [31,57]. Although the integrated system achieved regulatory compliance for most target metal(loid)s, including Cu, Cd, Zn, and As, residual nickel under T2 conditions at 30-day HRT (ranging between 130 and 830 μg L^{-1}) exceeds the 40 μg L^{-1} Flemish groundwater limit, despite a >99.9% reduction relative to raw groundwater (186.6 mg L^{-1}). Nickel exhibited greater persistence than copper (264.0 mg L^{-1} reduced to <6 μg L^{-1}) or zinc (98.1 mg L^{-1} reduced to <5 μg L^{-1}). While *P. australis* and *T. angustifolia* mesocosms operating under T2 conditions at 30-day HRT significantly reduce acute metal and metalloid toxicity, meeting this regulatory compliance threshold for nickel would necessitate extended HRTs or additional polishing steps.

Despite the promising performance achieved, the progressive loss of bioelectrochemical activity observed throughout treatment represents the main limitation of the system and highlights the need for improvements in long-term operational stability. As a first assessment of the feasibility of sequentially coupling BES treatment with phytoremediation, the present study does not aim to establish a fully integrated treatment technology but rather demonstrates the potential complementarity of two standalone technologies operated in sequence. The outcomes of this work therefore provide a basis for further development and optimization of the proposed treatment strategy, particularly with regard to the factors governing its long-term stability. Future research should therefore focus on (i) evaluating alternative reactor configurations, such as incorporating additional chambers or selective

membrane arrangements, or continuous anolyte renewal strategies to maintain favorable conditions for bioanode activity and facilitate biofilm reactivation using organic media, (ii) implementing dynamic voltage control strategies in MEC operation to optimize the sequential recovery and removal of different metal(loid)s according to their electrochemical characteristics, and (iii) systematically investigating critical operational parameters, such as membrane fouling, electrode passivation, oxygen leakage, and evaporation losses, together with appropriate mitigation strategies, including targeted chemical backwashing protocols.

Addressing these operational aspects will be essential to sustain BES performance over extended treatment. In addition, a limitation of the present work is the absence of direct mineralogical and surface spectroscopy (such as SEM-EDS, XRD, and/or FTIR) to characterize the solid-phase precipitates formed on the cathode and membrane surfaces. Future investigations should therefore incorporate advanced surface characterization to elucidate the relative contributions of electrodeposition versus chemical precipitation and complexation, thereby providing experimental evidence to support or refine the mechanistic interpretations proposed in the present study.

5. Conclusions

The sequential BES treatment achieved an overall metal(loid) removal efficiency of 91%, with near-complete removal of Cu and Fe (>99%) during the MFC stage, while the subsequent MEC stage enabled the efficient removal of Al (92%), As (90%), Cd (87%), Zn (76%), and Ni (71%). Simultaneously, BES operation increased groundwater pH values from 2.66 to 4.65, reducing metal mobility and improving the suitability of the treated water for subsequent biological polishing. The phytoremediation stage successfully treated the remaining contaminants and the exhausted anolyte streams generated by BES operation. The residual concentrations for most of target metal(loid)s, including Cu, CD, Zn, and As, in the wetland effluents were reduced to levels below the Flemish groundwater sanitation standards. Although nickel underwent a >99.9% concentration reduction, residual Ni levels remained above the 40 μg L^{-1} regulatory limit. Simultaneously, nutrient concentrations and ecotoxicological impacts were also significantly reduced. The *A. fischeri* bioluminescence assay confirmed a substantial reduction in toxicity following the combined BES–phytoremediation treatment. Among the tested species, *P. australis* and *S. holoschoenus* exhibited the highest tolerance and biomass production under exposure to BES-treated water and are therefore considered the most suitable candidates for future scale-up applications. The proposed treatment system reduces contaminant loads prior to plant exposure, improves operational flexibility, allows the valorization of exhausted anolyte streams, and maximizes the complementary strengths of each technology. The results therefore provide new evidence supporting the use of integrated bioelectrochemical and nature-based solutions for complex groundwater remediation. Overall, the results demonstrate that the integration of BESs and phytoremediation constitutes a promising next-generation nature-based remediation strategy capable of addressing complex metal(loid)-contaminated groundwater while simultaneously improving water quality, reducing toxicity, and promoting more circular management of treatment by-products.

Supplementary Materials: The following supporting information can be downloaded at: https://www.mdpi.com/article/10.3390/w18202574/s1, details for the composition of acetate mineral medium (ABBM) used in this study, and Table S1: Physico-chemical parameters of water monitored at different HRTs in macrophytes mesocosms.

Author Contributions: Conceptualization, A.H.A.K., M.A., E.B. and R.B.; Methodology, A.H.A.K., A.S.-C., M.A., C.R. (Carlos Rumbo), D.M. and P.B.-J.; Software, A.H.A.K., M.A., A.S.-C. and A.P.-d.-M.; Validation, A.H.A.K., D.L., S.d.l.P., C.R. (Carlos Rad) and E.B.; Formal Analysis, A.H.A.K., A.S.-C., M.A., C.R. (Carlos Rumbo), S.d.l.P., B.V.-A., P.B.-J. and H.D.W.; Resources, C.R. (Carlos Rad), C.R. (Carlos Rumbo), E.B. and R.B.; Data Curation, A.H.A.K., A.S.-C., M.A., D.L., C.R. (Carlos Rad) and A.P.-d.-M.; Writing—Original Draft Preparation, A.H.A.K., M.A., D.L., E.B. and R.B.; Writing—Review and Editing, A.H.A.K., C.R. (Carlos Rad), C.R. (Carlos Rumbo), M.A., D.L., E.B. and R.B.; Visualization, A.H.A.K., M.A., S.d.l.P. and D.L.; Supervision, A.H.A.K., E.B. and R.B.; Project Administration, A.H.A.K., E.B., B.V.-A. and R.B.; Funding Acquisition, A.H.A.K., B.V.-A., E.B. and R.B. All authors have read and agreed to the published version of the manuscript.

Funding: The authors want to acknowledge the funding received under the GREENER and BIOSYSMO projects. The GREENER project has received funding from the European Union's Horizon 2020 research and innovation program under the Grant Agreement No. 826312, while the BIOSYSMO project is funded by the European Union under the Grant Agreement No. 101060211. AS and SP have a predoctoral grant from Junta de Castilla y León, ORDEN EDU/842/2022, of the 6th of July, and ORDEN EDU/1009/2024, of the 10th of October, respectively.

Data Availability Statement: The original contributions presented in this study are included in the article and Supplementary Material. Further inquiries can be directed to the corresponding author(s).

Acknowledgments: The authors would like to thank the Editorial Office of Water for granting the full waiver for this manuscript.

Conflicts of Interest: Martí Aliaguilla, Diana Losantos, Daniele Molognoni, Pau Bosch-Jimenez, and Eduard Borràs were employed by the company Leitat Technological Center. Herwig De Wilde and Alfredo Pérez-de-Mora were employed by the company TAUW België nv and TAUW GmbH, respectively. The remaining authors declare that the research was conducted in the absence of any commercial or financial relationships that could be construed as potential conflicts of interest.

References

1. Ahmad, T.; Usman, M.; Almeetani, M.; Ahmed, A.; Qadir, A.; Hakeem, M.K.; Shah, I.; Iltaf, K.H. Heavy Metal(Loid) Contamination in Groundwater of the Eastern Salt Range, Pakistan: Source Apportionment and Ecological-Human Health Risk Assessment. *Earth Syst. Environ.* **2026**, *10*, 11335–11363. [CrossRef]
2. Roy, R.; Saha, R.P. Global Insights into Heavy Metal Contamination of Groundwater and Approaches for Sustainable Remediation. *Biol. Bull. Rev.* **2026**, *16*, 822–848. [CrossRef]
3. Velasco-Arroyo, B.; Curiel-Alegre, S.; Khan, A.H.A.; Rumbo, C.; Pérez-Alonso, D.; Rad, C.; De Wilde, H.; Pérez-de-Mora, A.; Barros, R. Phytostabilization of Metal(Loid)s by Ten Emergent Macrophytes Following a 90-Day Exposure to Industrially Contaminated Groundwater. *N. Biotechnol.* **2024**, *79*, 50–59. [CrossRef] [PubMed]
4. Hussain, N.; Asif, M.; Shafaat, S.; Khan, M.S.; Riaz, N.; Iqbal, M.; Javed, A.; Butt, T.A.; Shaikh, A.J.; Bilal, M. Multilayer Adsorption of Reactive Orange 16 Dye onto Fe_2O_3/ZnO Hybrid Nanoadsorbent: Mechanistic Insights from Kinetics, Isotherms and Dynamic Light Scattering Studies. *J. Chem. Technol. Biotechnol.* **2025**, *100*, 50–66. [CrossRef]
5. Rajan, M.; Karunanidhi, D.; Jaya, J.; Preethi, B.; Subramani, T.; Aravinthasamy, P. A Comprehensive Review on Human Health Hazards Due to Groundwater Contamination: A Global Perspective. *Phys. Chem. Earth* **2024**, *135*, 103637. [CrossRef]
6. Ehsan, N.; Dawood, A.; Waheed, F.; Nasir, R.; Rebouh, N.Y.; Rizvi, S.I.; Muzamil, A.; uz Zaman, Q. Human and Ecological Health Risks from Heavy Metal Contamination in Groundwater Aquifers. *Sci. Rep.* **2025**, *15*, 22826. [CrossRef] [PubMed]
7. Khan, A.H.A.; Budzyńska, S.; Zine, H.; Vázquez-Núñez, E.; Talpur, S.A.; Hassan, M.; Barros, R. Dendroremediation: A Sustainable Nature-Based Solution for Management of Abandoned Mining Sites and Brownfields. *J. Clean. Prod.* **2025**, *501*, 145342. [CrossRef]
8. Fareed, A.; Riaz, S.; Nawaz, I.; Iqbal, M.; Ahmed, R.; Hussain, J.; Hussain, A.; Rashid, A.; Naqvi, T.A. Immobilized Cells of a Novel Bacterium Increased the Degradation of N-Methylated Carbamates under Low Temperature Conditions. *Heliyon* **2019**, *5*, e02740. [CrossRef] [PubMed]
9. Türker, O.C.; Yakar, A. A Hybrid Constructed Wetland Combined with Microbial Fuel Cell for Boron (B) Removal and Bioelectric Production. *Ecol. Eng.* **2017**, *102*, 411–421. [CrossRef]
10. Mosquera-Romero, S.; Ntagia, E.; Rousseau, D.P.L.; Esteve-Núñez, A.; Prévoteau, A. Water Treatment and Reclamation by Implementing Electrochemical Systems with Constructed Wetlands. *Environ. Sci. Ecotechnol.* **2023**, *16*, 100265. [CrossRef] [PubMed]

11. Lian, Z.; Kong, F.-Y.; Lian, Z.; Kong, F. Treatments of Heavy Metals in Bio Electrochemical Systems (BES) and Microbial Transfer Mechanisms: Analyses of Influencing Factors, Future Research Directions, Prospect and Outlook. *Water Air Soil Pollut.* **2025**, *236*, 486. [CrossRef]
12. Liu, S.H.; Liu, J.S.; Lin, C.W. Heavy Metal Removal and Recovery from Contaminated Sediments Based on Bioelectrochemical Systems: Insights, Progress, and Perspectives. *Int. Biodeterior. Biodegrad.* **2025**, *196*, 105940. [CrossRef]
13. Li, Y.; Kong, D.; Jin, K.; Dong, X.; Zhang, Q.; Chen, L. Field Application of Bioelectrochemical Reduction Technology for Treating Hexavalent Chromium in Groundwater. *J. Contam. Hydrol.* **2026**, *276*, 104744. [CrossRef] [PubMed]
14. Dubois, E.; Loghmani-Khouzani, T.; Ottaviani, S.; Serrao, L.; Starkey, E. Are Water-Related Nature-Based Solutions (NbS) Assessed for Their Full Multi-Benefit Potential? A Review from an Urban Perspective. *Sustain. Nexus Forum* **2025**, *33*, 22. [CrossRef]
15. Khan, A.H.A.; Soto-Cañas, A.; Rad, C.; Curiel-Alegre, S.; Rumbo, C.; Velasco-Arroyo, B.; de Wilde, H.; Pérez-de-Mora, A.; Martel-Martín, S.; Barros, R. Macrophyte Assisted Phytoremediation and Toxicological Profiling of Metal(Loid)s Polluted Water Is Influenced by Hydraulic Retention Time. *Environ. Sci. Pollut. Res.* **2024**, *32*, 16760–16779. [CrossRef] [PubMed]
16. González-Méndez, L.M.; Martínez-Amador, S.Y.; Ríos-González, L.J.; Pérez-Rodríguez, P.; Perez-Rodríguez, M.A.; Reyes-Acosta, A.V.; Rodríguez-De la Garza, J.A. A Review on Anatomical and Physiological Traits of Aquatic Macrophytes Coupled to a Bioelectrochemical System: Comparative Wastewater Treatment Performance. *Processes* **2025**, *13*, 1545. [CrossRef]
17. Strycharz, J.; Nawrot, N.; Kowal, P.; Godzieba, M.; Matej-Łukowicz, K.; Szeląg, B.; Ciesielski, S.; Wojciechowska, E. Synergistic Integration of Floating Wetlands and Microbial Fuel Cells via Plant-Microbe-Electrode Interactions. *Ecol. Eng.* **2026**, *230*, 108041. [CrossRef]
18. Komunikasi, M.; Pengembangan, D.; Lingkungan, T.; Wahyuni, A.D.; Yuniarto, A.; Arliyani, I.; Min, B. Effect of Floating Plants on Constructed Wetland Microbial Fuel Cell Treating Domestic Wastewater. *J. Presipitasi.* **2025**, *22*, 980–992. [CrossRef]
19. Ingrid Maldonado, Y.M.R. Electrochemical Technologies and Phytoremediation: Strategies for Antibiotic Waste Removal, Electricity Generation, and Water Quality Improvement. *Environ. Eng. Res.* **2025**, *30*, 240677. [CrossRef]
20. Qian, H.; Gao, Z.; Sapsford, D.; Chen, W.; Huang, Q.; Harbottle, M. Synergistic Enhancement of Copper Recovery from Recalcitrant Mineral Phases by Plant Microbial Fuel Cells. *J. Hazard. Mater.* **2026**, *505*, 141421. [CrossRef] [PubMed]
21. Ancona, V.; Cavone, C.; Grenni, P.; Gagliardi, G.; Cosentini, C.; Borello, D.; Barra Caracciolo, A. Plant Microbial Fuel Cells for Recovering Contaminated Environments. *Int. J. Hydrogen Energy* **2024**, *72*, 1116–1126. [CrossRef]
22. Wang, S.; Adekunle, A.; Raghavan, V. Bioelectrochemical Systems-Based Metal Removal and Recovery from Wastewater and Polluted Soil: Key Factors, Development, and Perspective. *J. Environ. Manag.* **2022**, *317*, 115333. [CrossRef] [PubMed]
23. Mohrazi, A.; Ghasemi-Fasaei, R.; Mojiri, A.; Safarzadeh Shirazi, S. Investigating an Electro-Bio-Chemical Phytoremediation of Multi-Metal Polluted Soil by Maize and Sunflower Using RSM-Based Optimization Methodology. *Environ. Exp. Bot.* **2023**, *211*, 105352. [CrossRef]
24. Wang, X.X.; Zhao, Y.; Jin, L.; Liu, B. Performance and Mechanism of a Bioelectrochemical System for Reduction of Heavy Metal Cadmium Ions. *RSC Adv.* **2024**, *14*, 5390–5399. [CrossRef] [PubMed]
25. Khan, A.H.A.; Velasco-Arroyo, B.; Rad, C.; Curiel-Alegre, S.; Rumbo, C.; de Wilde, H.; Pérez-de-Mora, A.; Martel-Martín, S.; Barros, R. Metal(Loid) Tolerance, Accumulation, and Phytoremediation Potential of Wetland Macrophytes for Multi-Metal(Loid)s Polluted Water. *Environ. Sci. Pollut. Res.* **2024**, *31*, 65724–65740. [CrossRef] [PubMed]
26. Ibáñez, J.; Pérez-de-Mora, A.; Santiago-Herrera, M.; Belloncle, B.; de Wilde, H.; Martel-Martín, S.; Blanco-Alcántara, D.; Barros, R. Environmental and Socio-Economic Evaluation of a Groundwater Bioremediation Technology Using Social Cost-Benefit Analysis: Application to an in-Situ Metal(Loid) Precipitation Case Study. *Sci. Total Environ.* **2024**, *954*, 176720. [CrossRef] [PubMed]
27. Coetsiers, M.; Blaser, P.; Martens, K.; Walraevens, K. Natural Background Levels and Threshold Values for Groundwater in Fluvial Pleistocene and Tertiary Marine Aquifers in Flanders, Belgium. *Environ. Geol.* **2008**, *57*, 1155–1168. [CrossRef]
28. Bosch-Jimenez, P.; Martinez-Crespiera, S.; Amantia, D.; Della Pirriera, M.; Forns, I.; Shechter, R.; Borràs, E. Non-Precious Metal Doped Carbon Nanofiber Air-Cathode for Microbial Fuel Cells Application: Oxygen Reduction Reaction Characterization and Long-Term Validation. *Electrochim. Acta* **2017**, *228*, 380–388. [CrossRef]
29. Bosch-Jimenez, P.; Corbella, C.; Gaudes, A.; Sanchis, S.; Lopez, P.; Molognoni, D.; Villazán Cabero, A.; de Cuenca, J.M.; Borràs, E. Electrowetland Pilot of 50 M2: Operation and Characterization Under Real Conditions for 1 Year. *Fuel Cells* **2024**, *24*, e202300231. [CrossRef]
30. Khan, A.H.A.; Soto-Cañas, A.; Rad, C.; Martin-Pablo, A.; Velasco-Arroyo, B.; de la Fuente-Vivas, D.; Gómez-Cuadrado, L.; Salazar-Mardones, G.; De Wilde, H.; Pérez-de-Mora, A.; et al. Phragmites Australis and Scirpus Holoschoenus for Metal(Loid)s Polluted Groundwater Remediation: A Wetland Mesocosm Study with Different Exposure Regimes. *J. Hazard. Mater.* **2026**, *509*, 142030. [CrossRef] [PubMed]
31. Rumbo, C.; Bianchin, A.; Locci, A.M.; Barros, R.; Martel Martín, S.; Tamayo-Ramos, J.A. Toxicological Assessment of Nanocrystalline Metal Alloys with Potential Applications in the Aeronautical Field. *Sci. Rep.* **2022**, *12*, 1523. [CrossRef] [PubMed]
32. Xu, H.; Hou, D. Unlocking Nature-Based Solution Potential: Life Cycle Assessment of Groundwater Remediation at Operating Industrial Sites. *J. Clean. Prod.* **2025**, *528*, 146697. [CrossRef]

33. Bhattacharya, A.; Garg, S.; Chatterjee, P. Examining Current Trends and Future Outlook of Bio-Electrochemical Systems (BES) for Nutrient Conversion and Recovery: An Overview. *Environ. Sci. Pollut. Res.* **2023**, *30*, 86699–86740. [CrossRef] [PubMed]
34. Delgado, Y.; Llanos, J.; Fernández-Morales, F.J. Coupling of Electrodialysis and Bio-Electrochemical Systems for Metal and Energy Recovery from Acid Mine Drainage. *J. Chem. Technol. Biotechnol.* **2024**, *99*, 2178–2185. [CrossRef]
35. Pines Pozo, M.T.; Lopez Fernandez, E.; Villaseñor, J.; Leon-Fernandez, L.F.; Fernandez-Morales, F.J. Metal Recovery from Wastes: A Review of Recent Advances in the Use of Bioelectrochemical Systems. *Appl. Sci.* **2025**, *15*, 1456. [CrossRef]
36. Kim, C.; Song, Y.E.; Kong, D.S.; Kim, Y.; Lee, S.Y.; Yu, J.; Lee, T. Why Two-Chamber Microbial Fuel Cells Matter for Metal Recovery: Spatial and Temporal Separation Enables Spontaneous Metal Ion Reduction. *Desalination* **2026**, *637*, 120486. [CrossRef]
37. Modin, O.; Wang, X.; Wu, X.; Rauch, S.; Fedje, K.K. Bioelectrochemical Recovery of Cu, Pb, Cd, and Zn from Dilute Solutions. *J. Hazard. Mater.* **2012**, *235–236*, 291–297. [CrossRef] [PubMed]
38. Zhang, X.; Li, X.; Zhao, X.; Li, Y. Factors Affecting the Efficiency of a Bioelectrochemical System: A Review. *RSC Adv.* **2019**, *9*, 19748–19761. [CrossRef] [PubMed]
39. Sieber, A.; Spiess, S.; Rassy, W.Y.; Schild, D.; Rieß, T.; Singh, S.; Jain, R.; Schönberger, N.; Lederer, F.; Kremser, K.; et al. Fundamentals of Bio-Based Technologies for Selective Metal Recovery from Bio-Leachates and Liquid Waste Streams. *Front. Bioeng. Biotechnol.* **2024**, *12*, 1528992. [CrossRef] [PubMed]
40. Kim, J.G.; Kim, H.B.; Shin, D.H.; Alessi, D.S.; Kwon, E.; Baek, K. In-Situ Generation of Reactive Oxygen Species Using Combination of Electrochemical Oxidation and Metal Sulfide. *Sci. Total Environ.* **2021**, *789*, 147961. [CrossRef] [PubMed]
41. Zhang, P.; Karabulut, B.Y. Electrochemical Coagulant Generation via Aluminum-Based Electrocoagulation for Sustainable Greywater Treatment and Reuse: Optimization Through Response Surface Methodology and Kinetic Modelling. *Molecules* **2025**, *30*, 3779. [CrossRef] [PubMed]
42. Heidmann, I.; Calmano, W. Removal of Zn(II), Cu(II), Ni(II), Ag(I) and Cr(VI) Present in Aqueous Solutions by Aluminium Electrocoagulation. *J. Hazard. Mater.* **2008**, *152*, 934–941. [CrossRef] [PubMed]
43. Al Aji, B.; Yavuz, Y.; Koparal, A.S. Electrocoagulation of Heavy Metals Containing Model Wastewater Using Monopolar Iron Electrodes. *Sep. Purif. Technol.* **2012**, *86*, 248–254. [CrossRef]
44. Kosolapov, D.B.; Kuschk, P.; Vainshtein, M.B.; Vatsourina, A.V.; Wießner, A.; Kästner, M.; Müller, R.A. Microbial Processes of Heavy Metal Removal from Carbon-Deficient Effluents in Constructed Wetlands. *Eng. Life Sci.* **2004**, *4*, 403–411. [CrossRef]
45. Hidayat, A.R.P.; Widyanto, A.R.; Asranudin, A.; Ediati, R.; Sulistiono, D.O.; Putro, H.S.; Sugiarso, D.; Prasetyoko, D.; Purnomo, A.S.; Bahruji, H.; et al. Recent Development of Double Chamber Microbial Fuel Cell for Hexavalent Chromium Waste Removal. *J. Environ. Chem. Eng.* **2022**, *10*, 107505. [CrossRef]
46. Zeppilli, M.; Paiano, P.; Torres, C.; Pant, D. A Critical Evaluation of the PH Split and Associated Effects in Bioelectrochemical Processes. *Chem. Eng. J.* **2021**, *422*, 130155. [CrossRef]
47. Guo, F.; Luo, H.; Shi, Z.; Wu, Y.; Liu, H. Substrate Salinity: A Critical Factor Regulating the Performance of Microbial Fuel Cells, a Review. *Sci. Total Environ.* **2021**, *763*, 143021. [CrossRef] [PubMed]
48. Chakma, R.; Hossain, M.K.; Paramasivam, P.; Bousbih, R.; Amami, M.; Toki, G.F.I.; Haldhar, R.; Karmaker, A.K. Recent Applications, Challenges, and Future Prospects of Microbial Fuel Cells: A Review. *Glob. Chall.* **2025**, *9*, 2500004. [CrossRef] [PubMed]
49. Wu, X.; Xie, W.; Ye, J.; Sun, D.; Ohnuki, T.; Li, M.; Zhang, X.; Fang, Q.; Tang, Q.; Li, D. Progress in Heavy Metals-Containing Wastewater Treatment via Microbial Electrolysis Cell: A Review. *J. Water Process Eng.* **2023**, *55*, 104228. [CrossRef]
50. Yasri, N.; Roberts, E.P.L.; Gunasekaran, S. The Electrochemical Perspective of Bioelectrocatalytic Activities in Microbial Electrolysis and Microbial Fuel Cells. *Energy Rep.* **2019**, *5*, 1116–1136. [CrossRef]
51. Tiago, G.; Cristóvão, M.B.; Marques, A.P.; Huertas, R.; Merino-Garcia, I.; Pereira, V.J.; Crespo, J.G.; Velizarov, S. A Study on Biofouling and Cleaning of Anion Exchange Membranes for Reverse Electrodialysis. *Membranes* **2022**, *12*, 697. [CrossRef] [PubMed]
52. Fathima, A.; Ilankoon, I.M.S.K.; Zhang, Y.; Chong, M.N. Scaling up of Dual-Chamber Microbial Electrochemical Systems—An Appraisal Using Systems Design Approach. *Sci. Total Environ.* **2024**, *912*, 169186. [CrossRef] [PubMed]
53. Georg, S.; Schott, C.; Courela Capitao, J.R.; Sleutels, T.; Kuntke, P.; ter Heijne, A.; Buisman, C.J.N. Bio-Electrochemical Degradability of Prospective Wastewaters to Determine Their Ammonium Recovery Potential. *Sustain. Energy Technol. Assess.* **2021**, *47*, 101423. [CrossRef]
54. Greenman, J.; Gajda, I.; You, J.; Mendis, B.A.; Obata, O.; Pasternak, G.; Ieropoulos, I. Microbial Fuel Cells and Their Electrified Biofilms. *Biofilm* **2021**, *3*, 100057. [CrossRef] [PubMed]
55. Liang, Y.; Li, P.; Yang, W.; Huang, L.; Ji, Y.; Wang, X.; Zeng, X.; Xiang, H.; Ding, Y.; Feng, H. Innovative Sandwich Electrode-Assembled Bioelectrochemical System for Efficient Organic Pollutants Removal in Low-Conductivity Groundwater. *Water Res.* **2026**, *295*, 125557. [CrossRef] [PubMed]

56. Ai, C.; Hou, S.; Yan, Z.; Zheng, X.; Amanze, C.; Chai, L.; Qiu, G.; Zeng, W. Recovery of Metals from Acid Mine Drainage by Bioelectrochemical System Inoculated with a Novel Exoelectrogen, Pseudomonas Sp. E8. *Microorganisms* **2019**, *8*, 41. [CrossRef] [PubMed]
57. Connon, R.E.; Geist, J.; Werner, I. Effect-Based Tools for Monitoring and Predicting the Ecotoxicological Effects of Chemicals in the Aquatic Environment. *Sensors* **2012**, *12*, 12741–12771. [CrossRef] [PubMed]

Disclaimer/Publisher's Note: The statements, opinions and data contained in all publications are solely those of the individual author(s) and contributor(s) and not of MDPI and/or the editor(s). MDPI and/or the editor(s) disclaim responsibility for any injury to people or property resulting from any ideas, methods, instructions or products referred to in the content.